5.19

WARM WATER FORMATION IN THE MIDST OF THE SOUTHERN OCEAN

Sophie Wacongne[1], Kevin Speer
Florida State University, Tallahassee, Florida
Rick Lumpkin
Atlantic Oceanographic and Meteorological Laboratory, Miami, Florida
Vianney Sadoulet

Abstract

The global heat budget at southern high latitudes is thought to be dominated by heat and buoyancy loss, yielding intermediate or deep water formation. The net heat loss, however, is ill-known, not only because of poor observational coverage, but also because several climatologies of air-sea heat flux over the Southern Ocean show, imbedded in a large region of heat loss, bands of heat gain which could potentially reverse the global budget. One purpose of this work is to assess the significance of such heat gain. First we explore which of the parameters involved in the computation of the various components of air-sea heat flux can cause sign reversals of the net flux as one progresses poleward. We show that regions of net heat gain, typically near 50°S, coincide with regions of strong meridional gradients of sea surface temperature (SST). To the north, net heat loss results from net radiative gain offset by latent heat loss. To the south, net heat loss results from net short wave gain offset by net long wave loss. In between, values for evaporation and thus latent heat abruptly drop as SST drops, leaving the net short wave gain and the precipitation to dominate. Second we discuss whether a region of heat gain and the shallow upwelling cell with warm water formation that it would imply is compatible with what we know of the hydrography and oceanic circulation of the Southern Ocean. First we use an elementary two-dimensional box model of the upper Southern Ocean (zonally-integrated), then a three-dimensional box inverse model of the global ocean.

[1] *C*orresponding author address: Sophie Wacongne, Florida State University, Dept. of Oceanography, Tallahassee, F L 32306-4320; email: wacongne@ocean.fsu.edu

1 INTRODUCTION

Using da Silva et al.'s (1994) analysis of the COADS data set, Speer et al. (2000) found net heat and buoyancy gain near and south of the Polar Front (surface density near 27, average latitude 50–55°S), coincident with westerly winds, northward Ekman transport and Ekman pumping. They diagnosed a "diabatic Deacon cell" with southward import and upwelling of denser water from Upper Circumpolar Deep Water (UCDW) levels, and transformation into less dense water in the surface Ekman-driven northward limb. Heat and buoyancy loss prevails to the north (where Mode Waters are formed) and to the south (where the southward-flowing deeper North Atlantic Deep Water (NADW) levels are involved in a convective cell with the northward flowing Antarctic Bottom Water (AABW)). As reviewed by Speer et al. (2000), their shallow Deacon cell contrasts with alternate views of a deeper cell involving NADW (Toggweiler and Samuels, 1998; Dőős and Coward 1997; Webb and Suginohara, 2001) or of the absence of a cell following zonal integration along density layers (Dőős and Webb, 1994). On the other hand, it is compatible with the work of Karsten and Marshall (2002), who obtain a similar cell by estimating the residual circulation of the Antarctic Circumpolar Current (ACC) from observations of the surface Ekman transport and eddy field combined with gridded hydrographic data. In that work, surface buoyancy gain compatible with the one used by Speer et al. is inferred from the residual circulation and the surface buoyancy gradient. Our approach here is more basic: we go back to observed surface heat and freshwater gain estimates with the goal of assessing their robustness and deducing the possible depth and density range of the associated upwelling circulation.

2 HIGH LATITUDE HEAT GAIN

Over much of the ocean surface, the net air-sea heat flux tends to reflect the imbalance between the net short wave solar flux impinging the ocean surface and the latent heat flux leaving it, sensible heat flux and, to a lesser degree, net long wave flux being small. This is illustrated on Fig.1 with all heat flux components from NCEP 79-93 (see following section)

plotted between 70°S and 70°N using the same contour interval. As the net short wave flux (1c) diminishes poleward due to the sphericity of the earth surface, the relative importance of net long wave loss increases, and one thus expects, at the most elementary level, heat gain, warm temperatures and warm water formation at low latitude, heat loss, cold temperatures and cold water formation at high latitude. Locally, as discussed for instance by Hsiung (1986) for the global ocean at low and middle latitudes, regions of large net heating coincide with regions of cooler surface water where evaporative loss is reduced because cold air cannot hold as much moisture as warm air. As a consequence, the pattern of net oceanic heat flux tends to resemble the pattern of the ocean circulation, with warm currents loosing heat via enhanced evaporation and cold currents gaining heat via reduced evaporation. The most conspicuous region of tropical net heat gain is the eastern equatorial Pacific cold tongue (Fig.1a-b). However, heat gain is also apparent near 50°S above the cold Antarctic Circumpolar Current and, to a lesser extent, 50°N, at least in this data set. As one progresses toward 50°S, net heat gain in excess of 25 W m^{-2} appears where latent loss is reduced below 75 W m^{-2} in absolute value (see the equatorward limit of the southern shading in both 1a and 1b), and persists over the latitude range where short wave heat gain (1c) is still high compared to long wave loss (1d).

For a more quantitative assessment, meridional sections of all the heat flux components were extracted along 50°W (south of 30°S and north of 30°N), 90°W (south of 30°S) and 160°W (north of 30°N), i.e. through comparable bands of high latitude net heat gain in both hemispheres. Fig.2 shows the southern sections on the left (2a-c) and the northern sections of the right (2b-d), with latitude consistently from south to north. The short wave gain curves (thick dotted lines) thus tend to be mirror images of each other on Fig.2a-b and 2c-d, with values near 200 W m^{-2} at 30°S and 30°N decreasing quasi-linearly to about 50 W m^{-2} at 70°S and 70°N. Long wave heat loss (thin dotted) is almost constant everywhere, close to -50 W m^{-2}, so that the net radiative heat flux (short plus long wave, not shown) would be like short wave but translated down 50 W m^{-2}, remaining positive over the range of latitudes shown.

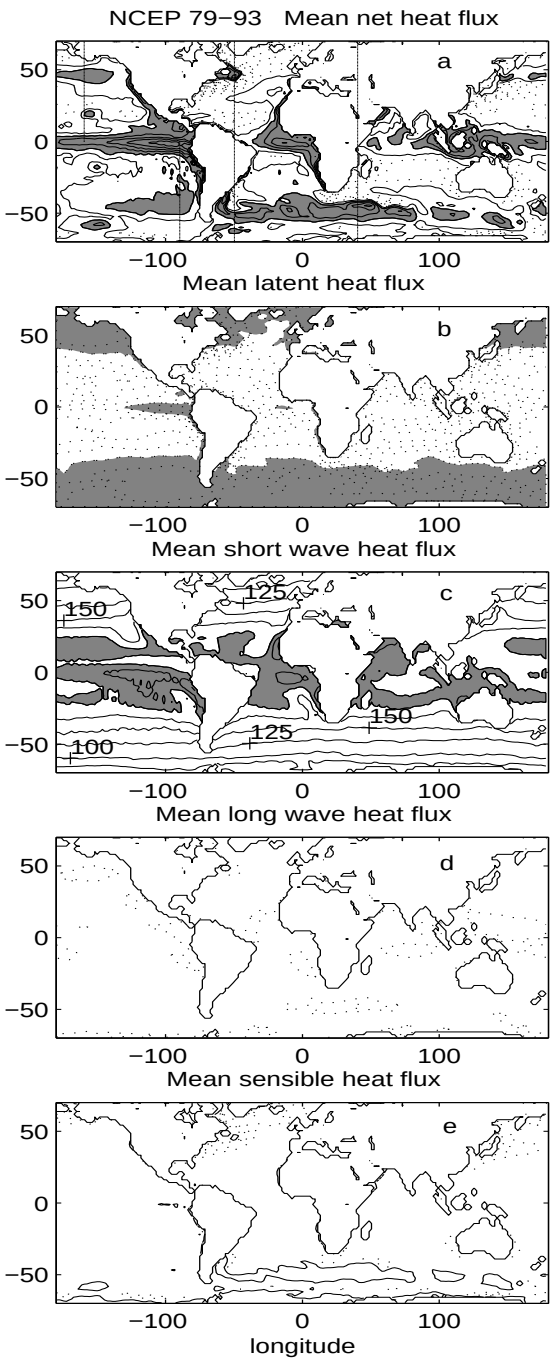

Figure 1: Net heat flux and its components between 70°S and 70°N from the NCEP 79-93 climatology. Contour interval is 25 W m^{-2} for all plots. Positive contours are solid, negative dotted. Shading indicates values greater than 25 W m^{-2} for net heat (1a), values less negative than -75 W m^{-2} for latent heat (1b), and values greater than 200 W m^{-2} for short wave (1c).

Within latitudes of net heat gain (thick solid, near 50–55 °S), sensible heat flux (thin dashed) is negligible compared to the other components. Equatorward of about 50°S and 50°N, latent heat flux (thick dashed) has a meridional gradient that controls that of net heat flux, while at higher latitudes all components can contribute equally.

The two upper panels (Fig.2a-b), representing the 50°W section in the western south and north Atlantic, show sharp meridional gradients of latent and net heat flux. These gradients are related to the ocean circulation in that the 50°W section lies close to the western coast where poleward subtropical warm western boundary currents collide with their equatorward subpolar cold counterparts (Brazil/Falkland and Gulf Stream/Labrador current systems). They are moreover influenced by the atmospheric circulation as evaporation is enhanced by dry continental westerlies blowing over warm waters (sensible heat loss is also enhanced and thus contributes to the net heat loss there). In contrast, the two bottom panels (Fig.2c-d) represent sections spanning qualitatively similar patterns of net heat gain in the southeastern and northeastern Pacific (Fig.1a). Both show quantitatively similar (relatively weak) meridional gradients of latent heat flux and quantitatively similar (moderate) values of net heat gain at comparable latitudes. These patterns are only minimally influenced by the oceanic circulation (weak at such locations), or by the atmospheric circulation (already saturated westerlies encountering no substantial zonal surface temperature gradient).

Turning back to Fig.1a, it is worth emphasizing that continental influence is minimal over most of the Southern Ocean. Exceptions occur off the southeast coast of South America as discussed above and around Antarctica (not shown). On a global scale, the North Atlantic, with its very limited region of high latitude heat gain centered on the Grand Banks, is the exception. Only there does the region of high evaporation extend far poleward along the path of the relatively warm North Atlantic Drift Current (see Warren 1983 for consequences on North Atlantic and Pacific oceans salt budget and deep water formation). This is shown on Fig.1b by the equatorward edge of the shading (-75 W m^{-2} contour). Far enough to the north, latent heat is eventually reduced, but so is short wave gain,

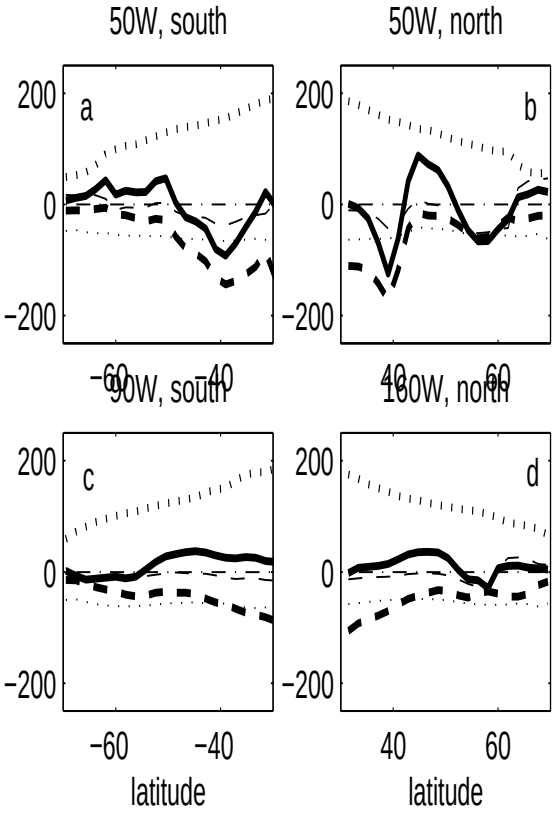

Figure 2: Meridional sections of mean net heat flux and its components from NCEP 79-93 along sections of Fig.1. Net is thick solid, short wave dotted, long wave thin dotted, latent thick dashed and sensible thin dashed, all in W m^{-2}. Left panels (a-c) concern the southern hemisphere, right panels the northern hemisphere. Upper panels (a-b) concern the western Atlantic, lower panels (c-d) the eastern Pacific.

so that the net remains negative. Elsewhere, latent heat reaches -75 W m^{-2} near 45°S and 45°N, where net radiative gain still reaches 100 W m^{-2}, hence a net heat gain. While illustrating that a high latitude band of heat gain may be the rule rather than an anomaly, this discussion also illustrates how sensitive the budget is to the meridional distribution of net short wave and latent heat fluxes and to their exact value. Given typical 20 W m^{-2} error bars on various surface heat fluxes climatologies, it is likely that where one climatology shows net heat gain, another one may only show a local minimum in net heat loss.

A study of the monthly evolution of the net heat flux and its components at 40°E/30–70°S (not shown) confirms the essential role of latent heat. The net heat flux displays a strong seasonal variation, driven by that of the net short wave heat flux while, at least north of 65°S, the seasonal variation of all the other terms, including that of latent heat, is negligible by comparison. North of about 40°S, latent heat reaches values negative enough to strongly temper (during austral summer) or completely overcome (during the rest of the year) the net short wave gain, hence the negative net annual mean of Fig.1a. South of 40°S, latent heat has dropped to absolute values small enough that a positive annual mean can prevail between about 40 and 60°S. A line of almost year-round heat gain near 42°S coincides with the locus of the strongest meridional gradients in latent heat and SST, and that of the 12°C isotherm (not shown). During austral summer (November to January), the net heat flux near 50°S reaches values larger than 100 W m^{-2}, well above the observational uncertainty. Of relevance for water mass formation, however, is the value of the net climatological mean, which will be influenced by differences in the strength of the seasonal cycle between different climatologies.

A more detailed exploration of the relationship between meridional gradients of SST and latent heat flux (lHF) is now warranted since lHF is only an indirect function of SST. It depends on the difference in specific humidity ($q_a - q_s$) between the air at 10 m and the air at the sea surface, assumed to be saturated, on the (10 m) wind speed V, on the air density ρ_a, on the latent heat of evaporation L and on a transfer coefficient C_e (function of the stability

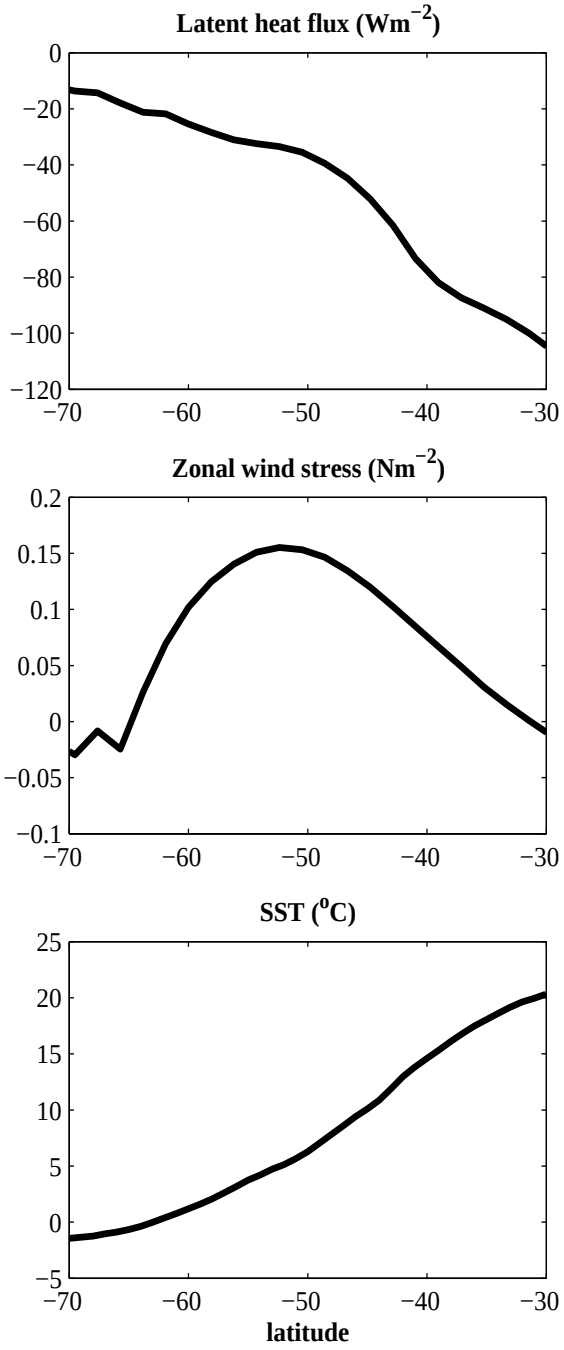

Figure 3: Meridional profiles of zonally-averaged latent heat flux (upper, from NCEP 79-93), zonal wind stress (middle, from NCEP 79-93) and SST (bottom, from SAC, see next section).

of the atmospheric surface layer), according to the bulk formula:

$$lHF = LE = LC_e\rho_a V(q_a - q_s)$$

with E the rate of evaporation. In practice, L, C_e and ρ_a display much less spatial variability than V or $(q_a - q_s)$ on long time scales, and SST and its meridional gradient influence lHF mostly via V and $(q_a - q_s)$.

A strong meridional gradient of SST implies a strong air temperature gradient, a strong zonal wind stress, and thus a tendency for linear enhancement of lHF as one progresses poleward into regions of stronger wind. However, as the air at the sea surface becomes colder and colder, it can hold less and less humidity: q_s is proportional to the saturation vapor pressure which decreases exponentially with temperature. The difference $|q_a - q_s|$ then drops (even though the specific humidity at 10 m q_a is likely to decrease too), hence a tendency for the rate of evaporation and thus $|lHF|$ to drop. Meridional profiles of zonally-averaged latent heat flux, zonal wind stress and SST (Fig.3) illustrate that the damping effect of reduced $|q_a - q_s|$ due to reduced SST wins over the enhancing effect of stronger wind.

3 INTERCOMPARISON OF CLIMATOLOGIES

For the purpose of intercomparing surface fluxes, we used several products:
- UWM/COADS (da Silva et al., 1994), over 1945-1989 (hereafter COADS)
- NCEP/NCAR, over 1948-2001 (hereafter NCEP 48-01)
- a subset of NCEP/NCAR over 1979-1993 (hereafter NCEP 79-93)
- a subset of ERA15/ECMWF over 1979-1993 (hereafter ECMWF 79-93)[2]
- SOC/COADS (Josey et al., 2002), over 1980-1993–we show below the adjusted October 2002 release– (hereafter SOC)

We also used the 3-D oceanic climatology from SAC/Hamburg (Gouretski and Jancke, 1998; hereafter SAC).

As revealed from horizontal maps of the various mean climatologies (not shown), all show

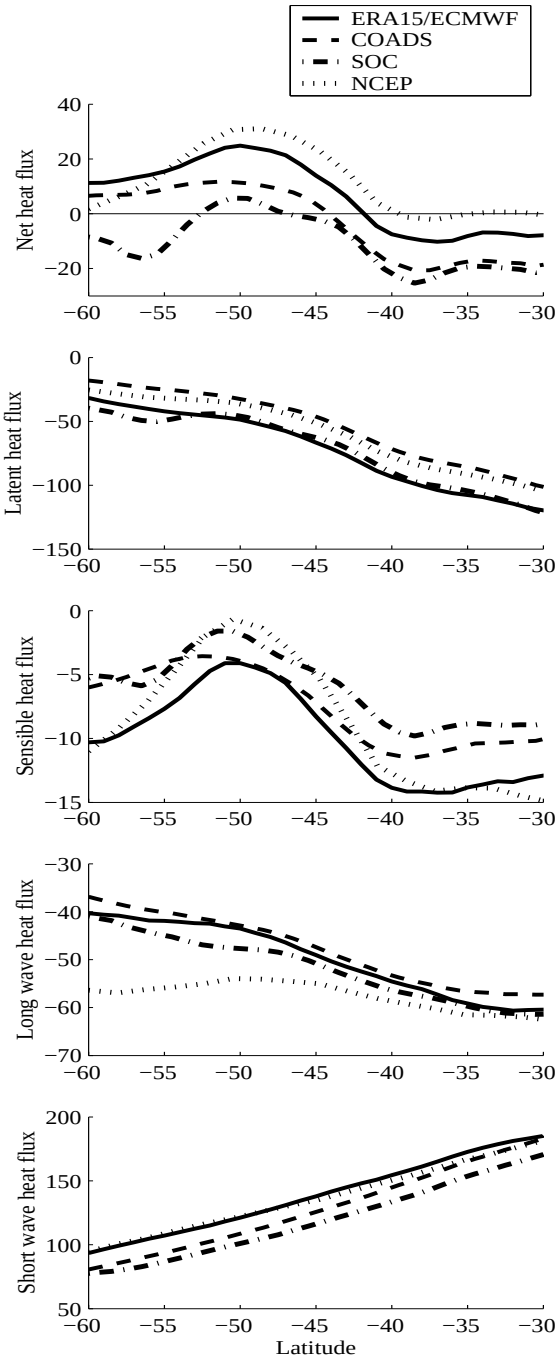

Figure 4: Meridional profiles of zonally-averaged net heat flux and its components from various climatologies

[2]both 79-93 climatologies courtesy of Laboratoire des Ecoulements Géophysiques et Industriels, Institut de Mécanique de Grenoble, France

qualitatively similar regions of net heat gain near 50°S, all linked to the sudden drop in evaporation rate accompanying the sudden drop in SST as one progresses poleward. And as revealed from annual mean meridional profiles of all components along 90°W, 50°W and 40°E from all the climatologies (not shown), similar balances between the various heat flux components hold in similar latitudinal ranges. As expected, however, there are substantial quantitative differences, as illustrated by the meridional profiles of the zonally-averaged net heat flux and its components (Fig.4). In particular, only in ECMWF and NCEP is the mean net heat flux at 50°S larger than 20 W m^{-2}. It is closer to 10 W m^{-2} in COADS and, while it was similar to ECMWF in SOC's earlier release (not shown), it has become only marginally positive in the latest one plotted here. The mean net heat flux at 50°S is larger in ECMWF and NCEP not because of smaller losses but because of a larger short wave gain. NCEP actually has a larger long wave loss than other products in this latitude range, and ECMWF tends to have a larger latent heat loss.

While this confirms the sensitivity of the heat budget over the Southern Ocean, and the need for better fluxes, what precedes still leads us to believe that localized heat gain is likely. Another way to confirm or infirm the occurence of mean net heat gain is to investigate its compatibility with the ocean circulation. Given the uncertainties in the values of the atmospheric fluxes, we first consider a very elementary ocean box model.

4 TWO-DIMENSIONAL OCEAN BOX MODEL

Just as one may link mean surface buoyancy loss to the strength and vertical extent of a mean meridional overturning cell, we will link mean surface buoyancy gain to the strength and vertical extent of a basic mean meridional upwelling circulation, to see whether the existence of such a circulation is compatible with what we know of the Southern Ocean. The approach is in the spirit of Warren (1983). Warren (1983) considers a box model of the upper North Pacific, imposes known values of the evaporation rate, subsurface salinity and horizontal transports, and deduces the surface salinity. We consider a box model for a wedge of the upper Southern Ocean,

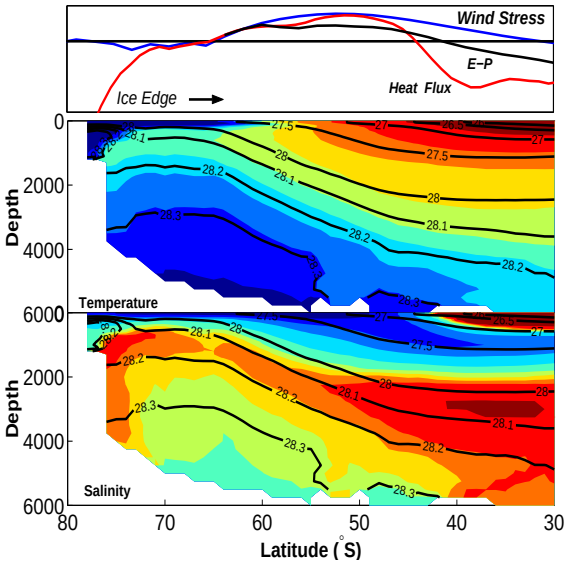

Figure 5: Zonally-averaged meridional section of T (upper) and S (lower) from SAC, along with rescaled profiles of the air-sea fluxes.

impose known values of the surface temperature and salinity, of the atmospheric fluxes and of the surface transport, and deduce subsurface temperature and salinity values, and hence vertical scales of the circulation.

Fig.5 shows a zonally-averaged meridional section of the oceanic temperature and salinity fields (using the SAC climatology), over which (rescaled) zonally-averaged meridional profiles of net heat flux, freshwater flux and zonal wind stress are plotted. At high latitudes, one expects bottom water formation within a deep overturning cell. North of about 65°S, isopycnals slope downward to the north, supporting geostrophic balance of the zonal ACC, and zonal wind stress and hence meridional Ekman transport are positive until close to 30°S. North of about 45°S, net heat, freshwater and hence buoyancy fluxes are negative, zonal wind stress decreases equatorward yielding Ekman pumping ($w_E = \partial V_E/\partial y < 0$), so oceanic fluxes support the concept of cold water formation and sinking along the downward sloping isolines. Between about 65°S and 45°S, net heat, freshwater and hence buoyancy fluxes are positive, and between about 65°S and 50°S (poleward of the westerly wind stress maximum), there is Ekman

upwelling. We are therefore going to assume an upwelling circulation in that region, disconnected from the deep overturning cell below and to the south. Within that upwelling region, relatively cold subsurface water flows southward and upward along the isopycnal surfaces and water lighter than, say, $\gamma = 28$ (the limit between UCDW and NADW) is transformed into warmer surface water carried northward by the Ekman transport, as represented schematically on Fig.6.

In such a two-layer model, and provided lateral diffusion is ignored, meridional heat transport equals net surface heat gain according to the equation:

$$HT(y) = \int\int_{65S}^{y} netHF(x, y')\, dy'\, dx$$

Zonal integrations are circumpolar, $HT(65°\mathrm{S})$ is taken to be zero because $V_E(65°\mathrm{S}) = 0$. Furthermore:

$$HT(y) = \rho c_p \left[V_1(y)\theta_1(y) + V_2(y)\theta_2(y)\right]$$

with (V_1, V_2) and (θ_1, θ_2) the upper and lower layer volume transports and potential temperatures respectively. We are assuming over the extent of the box model a constant value of the product ρc_p of the water density by its specific heat. Taking the upper layer meridional volume transport V_1 equal to the zonally-integrated meridional Ekman transport $V_E(y)$ and imposing no net transport through the northern section of the box ($V_2 = -V_1$), which amounts to neglecting the heat flux arising from the temperature difference between surface water and precipitation, one gets:

$$HT(y) = \rho c_p\, \Delta\theta\, V_E(y) = \rho c_p\, \Delta\theta \int \frac{-\tau^x(x, y)}{\rho_0 f}\, dx.$$

$\Delta\theta$ is the temperature difference $(\theta_1 - \theta_2)$ between upper and lower layer. From these two equations, $\Delta\theta$ can be calculated as a function of y as:

$$\Delta\theta(y) = \frac{1}{\rho c_p V_E} \int\int_{65S}^{y} netHF\, dy'\, dx$$

and θ_2 as:

$$\theta_2(y) = \Delta\theta(y) - \theta_1(y)$$

taking for $\theta_1(y)$ the value of the zonally-averaged climatological surface temperature.

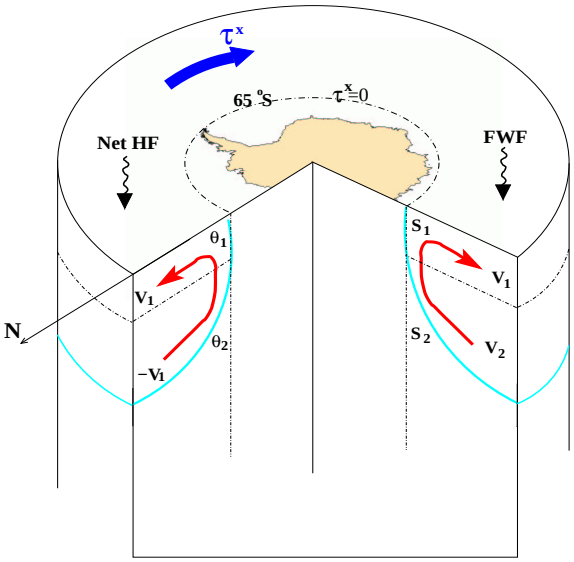

Figure 6: Schematic representation of our Southern Ocean wedge two-layer box model. Notations for the heat-driven circulation on the left, notations for the salt-driven circulation on the right. τ^x refers to the zonal wind stress.

Likewise, defining the net surface fresh water gain as:

$$FWF(y) = \int\int_{65S}^{y} (P - E)(x, y')\, dy'\, dx$$

with P the precipitation and E the evaporation rates, the freshwater and salt budgets yield the two equations:

$$V_2(y) = -V_1(y) - FWF(y)$$

$$V_1(y)S_1(y) + V_2(y)S_2(y) = 0.$$

Taking again for V_1 the zonally-integrated $V_E(y)$, and for S_1 the zonally-averaged climatological surface salinity, we can solve for the subsurface salinity:

$$S_2(y) = \frac{V_E(y)\, S_1(y)}{V_E(y) + FWF(y)}.$$

Having determined $\theta_2(y)$ and $S_2(y)$, we can then scan the zonally-averaged climatological sections of θ and S to see whether such values are encountered at all and, if so, determine their depth. Assuming our estimates of $\theta_2(y)$ and $S_2(y)$ provide depths compatible with each other

and with the climatological profiles, we thus obtain a rough estimate of the depth scale of our hypothetical upwelling cell. The procedure is crude. Differences in air-sea fluxes imply differences in the estimates of $\Delta\theta$ and S_2, in addition the choice of the climatological surface values and vertical T and S profiles influences the estimates of θ_2, S_2 and their depth. Moreover the estimate of the depth from the heat budget is made more delicate by the fact that the stratification is weak (so that a small difference in $\Delta\theta$ may yield a large difference in the depth of θ_2), and often capped by a temperature inversion.

Fig.7 shows the results obtained from both the heat budget and the salt budget of our simple two-layer model. South of 45°S, the results are actually more compatible than one might have expected, considering all the uncertainties involved and our oversimplication of the oceanic circulation. At 50°S, most estimates place the subsurface layer between 600 and 1500m, i.e. according to Fig.5, above $\gamma = 28$ and hence above NADW.

5 THREE-DIMENSIONAL INVERSE MODEL

Finally we consider the Southern Ocean box of an inverse model of the global ocean, built following Lumpkin and Speer's (2003) inverse model of the North Atlantic. The Southern Ocean box is bounded by the 32°S WOCE sections in the Atlantic, Pacific and Indian, and includes a circumpolar section (WOCE S4). Isopycnal and diapycnal transports are inferred from property budgets within isopycnal oceanic layers and air-sea fluxes binned as a function of density (rather than geographically as above). We consider the air-sea fluxes after inversion for two cases in which either 1) observed or 2) no air-sea fluxes were imposed a priori. Observed air-sea forcing is calculated from NCEP and COADS, using the mean from these two products as the prior forcing, and their difference as the magnitude of adjustments. The model also adjusts reference velocities and diapycnal mixing at layer interfaces. Mass, heat and salt are conserved in layers. Across S4, the interface γ=28.31 is chosen as the prior thermal wind reference level for the entire section, and the net volume and salt transports are constrained to $0 \pm 1{\times}10^6$ m^3 s^{-1} and 0 ± 35 psu $\times$

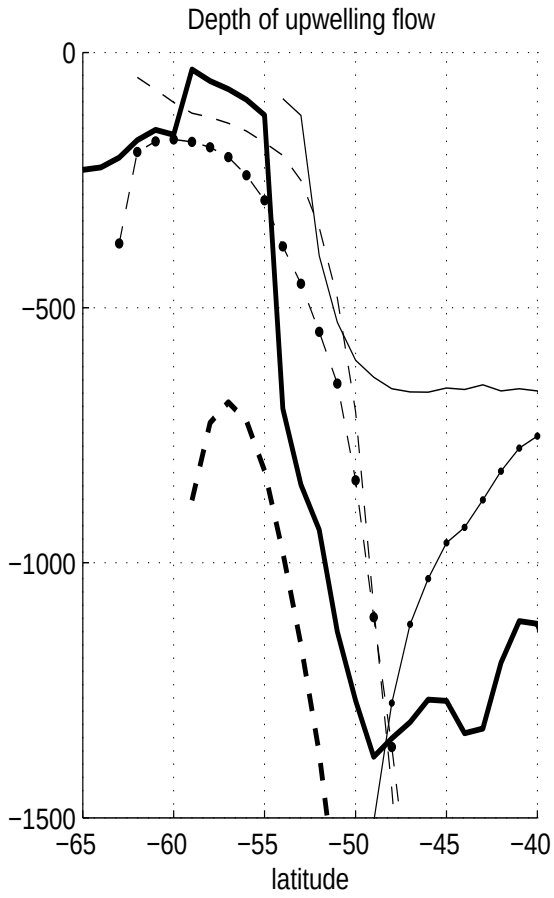

Figure 7: Meridional profiles of the depths associated with either the lower layer temperature of the elementary two-layer ocean model or its salinity, using various climatologies of air-sea fluxes and the SAC climatology for surface values and vertical profiles. Solid lines are depth profiles obtained from the heat budget, dashed lines are from the salt budget. Thin lines are from NCEP 48-01, thin lines with circles from ECMWF, thick lines from NCEP 79-93.

$\times 10^6$ m^3 s^{-1} respectively.

The inverse box model produces after inversion a region of heat and freshwater gain whether or not such gains were imposed a priori. Error bars are naturally larger in the case of the inversion without a priori air-sea fluxes, and indeed too large for the freshwater flux to be significantly positive. But the heat flux is always at least marginally positive near γ=27, the density surfacing near 50°S. This confirms that heat gain near 50°S is needed for compatibility with the observed hydrography and its associated circulation.

6 CONCLUSION

Our work suggests that heat gain, as present in several climatological products, and warm water formation are likely to occur near 50°S
- because this latitude band is characterized by relatively high values of radiative heat flux coexisting with a strong meridional SST gradient that causes reduced evaporation and latent heat loss,
- and because it appears to be consistent with the Southern Ocean hydrography and associated circulation, whether one considers a very elementary 2-D ocean box model or a more sophisticated 3-D inverse box model.
Another conclusion of this work is that, at first order, Southern Ocean upwelling may draw subsurface water from UCDW levels but probably very little from NADW levels.

Acknowlegements This paper summarizes Vianney Sadoulet's final year project for Ecole Centrale de Lyon, France. Help from Laurence Crosnier in gathering data products, and help from Nicolas Wienders in updating climatologies and producing figures is gratefully acknowledged.

References

da Silva, A.M., C.C. Young, and S. Levitus, 1994: Atlas of Surface Marine Data 1994. Vo.3: Anomalies of Heat and Momentum Fluxes. NOAA Atlas NESDIS 8, U.S. Department of Commerce, NOAA, NESDIS.

Dőős, K. and A. Coward, 1997: The Southern Ocean as the major upwelling zone of North Atlantic Deep Water. *Int. WOCE Newlett.*, 27, 3–4.

Dőős, K. and D.J. Webb, 1994: The Deacon Cell and the other meridional cells of the Southern Ocean. *J. Phys. Oceanogr.*, 24, 429–442.

Gouretski, V. and K. Jancke, 1998: A new world ocean climatology: Objective analysis on neutral surfaces. WOCE Rep.256/17, World Ocean Circ. Exp. Hydrogr. Progr. Spec. Anal. Cent., Hamburg, Germany.

Hsiung, J., 1986: Mean surface energy fluxes over the global ocean. *J. Geophys. Res.*, 91 C9, 10,585–10,606.

Josey, S.A., C. Kent, and P.K. Taylor, 2002: On the wind stress forcing of the ocean in the SOC climatology: Comparisons with the NCEP/NCAR, ECMWF, UWM/ COADS and Hellerman and Rosenstein datasets. *J. Phys. Oceanogr.*, 32, 1993–2019.

Karsten, R.H. and J. Marshall, 2002: Constructing the residual circulation of the ACC from observations. *J. Phys. Oceanogr.*, accepted.

Lumpkin, R., and K. Speer, 2003: Large-scale vertical and horizontal circulation in the North Atlantic Ocean. *J. Phys. Oceanogr.*, accepted.

Speer, K., S.R. Rintoul and B. Sloyan, 2000: The Diabatic Deacon Cell. *J. Phys. Oceanogr.*, 30, 3212-3222.

Toggweiler, J.R. and B. Samuels, 1998: On the ocean's large-scale circulation near the limit of no vertical mixing. *J. Phys. Oceanogr.*, 28, 1832-1852.

Warren, B.A. 1983: Why is no deep water formed in the North Pacific? *J. Marine Res.*, 41, 327–347.

Webb, D.J. and N. Suginohara, 2001: Vertical mixing in the ocean. *Nature*, 409, 37.